

Annealing-based approach to solving partial differential equations

Kazue Kudo*

*Department of Computer Science, Ochanomizu University, Tokyo 112-8610, Japan and
Graduate School of Information Sciences, Tohoku University, Sendai 980-8579, Japan*

(Dated: June 26, 2024)

Solving partial differential equations using an annealing-based approach is based on solving generalized eigenvalue problems. When a partial differential equation is discretized, it leads to a system of linear equations (SLE). Solving an SLE can be expressed as a general eigenvalue problem, which can be converted into an optimization problem with the objective function being a generalized Rayleigh quotient. The proposed algorithm allows the computation of eigenvectors at arbitrary precision without increasing the number of variables using an Ising machine. Simple examples solved using this method and theoretical analysis provide a guideline for appropriate parameter settings.

I. INTRODUCTION

Partial differential equations (PDEs) appear in various fields of science and engineering and have many applications. Since PDEs do not generally have analytical solutions, computational approaches are essential for solving PDEs. PDEs for a practical problem often have an extensive system size and many variables, requiring enormous computational resources such as memory and time. To tackle the issue, several quantum algorithms with exponential speedups have been proposed [1, 2]. Those algorithms rely on a fault-tolerant quantum computer. Since a fault-tolerant quantum computer has yet to be realized in a practical manner, using those algorithms is currently an unrealistic choice. For near-term quantum computers, variational quantum algorithms (VQAs) are promising. Several VQAs for solving PDEs have been proposed [3–6].

Discretizing a PDE leads to a system of linear equations (SLE). There are several VQAs proposed for solving SLE [3–8]. The problem for solving an SLE can be expressed as a generalized eigenvalue problem. The VQA for a generalized eigenvalue problem deals with an optimization problem whose objective function is a generalized Rayleigh quotient. Solving optimization problems is also the field where quantum annealing has an advantage. There are annealing-based algorithms for solving eigenvalue problems [9–11].

In this paper, our focus is on the annealing-based approach to solving PDEs. We aim to evaluate our annealing-based method and provide a guideline in parameter settings. In an annealing-based approach, the solution of a PDE is expressed as a linear combination of binary variables. The number of binary variables, which depends on the precision of real variables and the mesh size of discretized equations, is crucial in both quantum and simulated annealing. The available variables in a quantum annealing machine are limited, and the performance of simulated annealing depends on the dimension of the solution space, i.e., the number of variables. Con-

sidering these dependencies, we aim to provide a clear and practical guideline on suitable parameter settings.

Our method is based on the algorithm proposed in Ref. [11]. With controlled precision, the algorithm aims to solve eigenvalue problems using the quadratic unconstrained binary optimization (QUBO) formulation. In a usual QUBO formulation, increasing the precision of real variables requires more binary variables. However, using the proposed algorithm, one can compute eigenvectors at arbitrary precision without increasing the number of variables, although more iterations are required. Another advantage of the algorithm is that the desired accuracy becomes available even if the performance of the annealing procedure is imperfect. This paper uses a modified algorithm debugging the original one.

When used with Ising machines, the proposed algorithm to solve PDEs can work as a promising PDE solver. Ising machines are special-purpose computers that can solve combinatorial optimization problems more efficiently than conventional computers. They have been realized by several kinds of devices, such as a quantum annealer [12], digital processors based on simulated annealing (SA) [13–19], those based on simulated bifurcation [20–23], and coherent Ising machines [24–28]. Although initially designed to solve combinatorial optimization problems, they have applications in various fields. This work contributes to adding a new application. In this paper, numerical simulations using SA show how the number of iterations scales with the number of variables, which agrees with our theoretical estimate. They will provide a guideline for setting parameters for efficient computing.

II. METHODS

A. Generalized eigenvalue problem

The problem considered here is described by the SLE that is obtained by discretizing a PDE, and it is expressed as

$$Ku = f, \quad (1)$$

* kudo@is.ocha.ac.jp

where K is a positive-definite matrix, and \mathbf{u} and \mathbf{f} are real vectors. Although the SLE can be defined in a complex space, we consider a real space for simplicity. The aim is to obtain the solution \mathbf{u} for given K and \mathbf{f} .

The SLE can be transformed into the form of the generalized eigenvalue problem, which is generally written as

$$A\mathbf{v} = \lambda B\mathbf{v}, \quad (2)$$

where A and B are symmetric matrices, and B is positive definite. Here, λ and \mathbf{v} are the generalized eigenvalue and eigenvector, respectively. In this case, the smallest generalized eigenvalue λ_{\min} is equivalent to the minimum generalized Rayleigh quotient:

$$\lambda_{\min} = \min_{\mathbf{w}} \frac{\mathbf{w}^\top A \mathbf{w}}{\mathbf{w}^\top B \mathbf{w}}, \quad (3)$$

where \mathbf{w} is a unit vector, and the vector \mathbf{w} that minimizes $(\mathbf{w}^\top A \mathbf{w})/(\mathbf{w}^\top B \mathbf{w})$ is the eigenvector \mathbf{v}_{\min} corresponding to λ_{\min} .

Here, we rewrite Eq. (1) as

$$\tilde{K}\mathbf{u} = \tilde{\mathbf{f}}, \quad (4)$$

where $\tilde{K} = K/\|\mathbf{f}\|$ and $\tilde{\mathbf{f}} = \mathbf{f}/\|\mathbf{f}\|$, so as $\tilde{\mathbf{f}}$ is a unit vector. Equation (4) can be formulated as

$$-\tilde{\mathbf{f}}\tilde{\mathbf{f}}^\top \mathbf{v} = \lambda \tilde{K}\mathbf{v}, \quad (5)$$

which is the same form as Eq. (2). Comparing Eq. (2) with Eq. (5), we have $A = -\tilde{\mathbf{f}}\tilde{\mathbf{f}}^\top$ and $B = \tilde{K}$. Since $-\tilde{\mathbf{f}}\tilde{\mathbf{f}}^\top$ is a rank-1 matrix, Eq. (5) has only one nonzero eigenvalue, and the other eigenvalues are zero. The nonzero eigenvalue is negative, and thus, it is the smallest eigenvalue λ_{\min} . Dividing both sides of Eq. (5) by $\tilde{\mathbf{f}}^\top \mathbf{v}_{\min}$, which is nonzero as $\lambda_{\min} \neq 0$, we have

$$\tilde{K} \left(-\frac{\lambda_{\min} \mathbf{v}_{\min}}{\tilde{\mathbf{f}}^\top \mathbf{v}_{\min}} \right) = \tilde{\mathbf{f}}. \quad (6)$$

Combining Eqs. (4) and (6) results in

$$\tilde{K} \left(\mathbf{u} + \frac{\lambda_{\min} \mathbf{v}_{\min}}{\tilde{\mathbf{f}}^\top \mathbf{v}_{\min}} \right) = \mathbf{0}. \quad (7)$$

Considering that \tilde{K} is positive definite, i.e., invertible, we obtain the solution of Eq. (5), which is written as

$$\mathbf{u} = -\frac{\lambda_{\min} \mathbf{v}_{\min}}{\tilde{\mathbf{f}}^\top \mathbf{v}_{\min}}. \quad (8)$$

B. Algorithm

Here, we review the core of the algorithm proposed in Ref. [11], aiming to solve the generalized eigenvalue problem,

$$A\mathbf{v} = \lambda B\mathbf{v}, \quad (9)$$

where $A \in \mathbb{R}^{n \times n}$ is a symmetric matrix, and $B \in \mathbb{R}^{n \times n}$ is a symmetric positive-definite matrix. We approximate the eigenvector $\mathbf{v} \in \mathbb{R}^n$ as $\mathbf{v} = (I_n \otimes \mathbf{p})\mathbf{q}$, where $\mathbf{p} = (-1, \frac{1}{2}, \frac{1}{2^2}, \dots, \frac{1}{2^{b-1}})$ and $\mathbf{q} = \{0, 1\}^{nb}$. The precision vector \mathbf{p} is a row vector, and b is the parameter determining the precision of an initial-guess solution. The explicit form of \mathbf{v} is shown as

$$\mathbf{v} = \begin{bmatrix} -1, \frac{1}{2}, \dots, \frac{1}{2^{b-1}} & 0 & \dots & 0 \\ 0 & -1, \frac{1}{2}, \dots, \frac{1}{2^{b-1}} & & \vdots \\ \vdots & & \ddots & 0 \\ 0 & \dots & 0 & -1, \frac{1}{2}, \dots, \frac{1}{2^{b-1}} \end{bmatrix} \mathbf{q}. \quad (10)$$

Each element of \mathbf{v} takes a discrete value in the range of $[-1, 1 - \frac{1}{2^{b-1}}]$.

This algorithm consists of two stages. In the first stage, we obtain an initial guess of the solution of precision $\frac{1}{2^{b-1}}$. In the second stage, an optimization procedure is performed iteratively with increasing precision.

1. Initial guess stage

In the initial guess stage, the following two steps are repeated until λ converges:

1. Obtain the tentative eigenvector given as

$$\mathbf{v}^* = \underset{\mathbf{v}}{\operatorname{argmin}} [\mathbf{v}^\top (A - \lambda B) \mathbf{v}]. \quad (11)$$

2. Update the tentative eigenvalue calculated as

$$\lambda = \frac{\mathbf{v}^{*\top} A \mathbf{v}^*}{\mathbf{v}^{*\top} B \mathbf{v}^*}. \quad (12)$$

The initial value of λ is as $\lambda = \mathbf{x}^\top A \mathbf{x}$, where \mathbf{x} is a random unit vector. Step 1 consists of several substeps. First, using an annealing-based approach, obtain the solution of the QUBO given as

$$\mathbf{q}^* = \underset{\mathbf{q}}{\operatorname{argmin}} [\mathbf{q}^\top (A - \lambda B) \mathbf{q}]. \quad (13)$$

Second, calculate an unnormalized eigenvector $\mathbf{v} = (I_n \otimes \mathbf{p})\mathbf{q}^*$. Third, normalize the vector and obtain the tentative eigenvector $\mathbf{v}^* = \mathbf{v}/\|\mathbf{v}\|$. The convergence of this type of optimization, i.e., inexact parametric algorithms for mixed-integer fractional programs, has been proved for a good approximation of the solution [29].

Several additional approaches to obtaining better solutions were proposed in Ref. [11]. However, they are a little complicated. Here, we focus on the most straightforward version.

2. Iterative descent stage

The formal objective function to be minimized in the iterative descent stage is $g(\mathbf{x}) = \mathbf{x}^\top (A - \lambda B)\mathbf{x}$. Its Taylor expansion around \mathbf{x}_0 is written as

$$g(\mathbf{x}) = g(\mathbf{x}_0) + \mathbf{d}^\top \nabla g(\mathbf{x}_0) + \frac{1}{2} \mathbf{d}^\top (\nabla^2 g(\mathbf{x}_0)) \mathbf{d} + O(\|\mathbf{d}\|^3), \quad (14)$$

where $\mathbf{d} = \mathbf{x} - \mathbf{x}_0$. Here, ∇g and $\nabla^2 g$ denote the gradient and Hessian of g , respectively, and given as

$$\nabla g = 2(A - \lambda B)\mathbf{x}, \quad (15)$$

$$\nabla^2 g = 2(A - \lambda B). \quad (16)$$

The main procedure in the iterative descent stage is to repeat the computation of \mathbf{d} that minimizes g and the update of $\mathbf{x}_0 \leftarrow \mathbf{x}_0 + t\mathbf{d}$, where t is real.

Now, we consider obtaining the eigenvector corresponding to a given eigenvalue λ . The difference vector that minimizes the objected function is approximately given by

$$\mathbf{d}^* = \underset{\mathbf{d}}{\operatorname{argmin}} [2\mathbf{v}^\top (A - \lambda B)\mathbf{d} + \mathbf{d}^\top (A - \lambda B)\mathbf{d}], \quad (17)$$

where \mathbf{v} is a tentative eigenvector. Since the eigenvector is supposed to be a unit vector, vector \mathbf{v} changes on the unit sphere. Therefore, the difference should be orthogonal to \mathbf{v} . Orthogonalizing \mathbf{d}^* , we obtain the adjusted difference vector $\mathbf{d} = \mathbf{d}^* - (\mathbf{v}^\top \mathbf{d}^*)\mathbf{v}$. For updating the eigenvector as $\mathbf{v} \leftarrow \mathbf{v} + t\mathbf{d}$, the parameter t is determined to minimize

$$g(\mathbf{v} + t\mathbf{d}) = (\mathbf{v} + t\mathbf{d})^\top (A - \lambda B)(\mathbf{v} + t\mathbf{d}). \quad (18)$$

This quadratic function of t has a minimum only if $\mathbf{d}^\top (A - \lambda B)\mathbf{d} > 0$; if not, we set $t = 1$. To enforce $t \geq 1$, we define the parameter as

$$t = \begin{cases} \operatorname{sgn}(b) \max\left(\frac{|b|}{a}, 1\right) & a > 0, \\ 1 & a \leq 0, \end{cases} \quad (19)$$

where $a = \mathbf{d}^\top (A - \lambda B)\mathbf{d}$ and $b = -\mathbf{v}^\top (A - \lambda B)\mathbf{d}$. When $t \geq 1$, $\mathbf{v} + t\mathbf{d}$ possibly overshoots the exact solution, resulting in a worse estimate of the eigenvector. Overshooting indicates that the discretized mesh size is not small enough to produce better solutions. In that case, the mesh size is scaled down instead of updating \mathbf{v} . When the mesh size reaches $\epsilon_0/2^{b-1}$, where ϵ_0 is the tolerance precision parameter, the algorithm terminates.

The above procedure enables the generalized eigenvalue problem to be solved with arbitrary precision in principle. The original algorithm proposed in Ref. [11] provides solutions better than single precision but worse than double precision. This issue relies on the condition for downscaling the mesh size. The failure to improve the solution may be caused by the poor performance of

an annealing procedure, even though overshooting does not occur. If this is the case, the mesh size decreases at every iteration without improving a solution. To avoid such a case, the annealing procedure should be iterated several times at the present mesh size when the solution shows no improvement.

The procedure in the iterative descent stage is summarized as follows. First, set the precision to an initial value: $r = r_{\text{init}}$. Then, the following procedure is repeated until r reaches ϵ_0 .

- (1) Using an annealing-based approach, obtain the solution of the QUBO given as

$$\mathbf{q}^* = \underset{\mathbf{q}}{\operatorname{argmin}} [2r\mathbf{v}^\top C(I_n \otimes \mathbf{p})\mathbf{q} + r^2 \mathbf{q}^\top (C \otimes \mathbf{p}^\top \mathbf{p})\mathbf{q}], \quad (20)$$

where $C = A - \lambda B$.

- (2) Obtain the adjusted difference vector $\mathbf{d} = \mathbf{d}^* - (\mathbf{v}^\top \mathbf{d}^*)\mathbf{v}$, where $\mathbf{d}^* = (I_n \otimes \mathbf{p})r\mathbf{q}^*$.
- (3) Calculate the tentative eigenvector as $\mathbf{v}_{\text{tnt}} = \mathbf{v} + t\mathbf{d}$, where t is defined by Eq. (19).
- (4) Update the tentative eigenvalue calculated as

$$\lambda_{\text{tnt}} = \frac{\mathbf{v}_{\text{tnt}}^*{}^\top A \mathbf{v}_{\text{tnt}}^*}{\mathbf{v}_{\text{tnt}}^*{}^\top B \mathbf{v}_{\text{tnt}}^*}. \quad (21)$$

- (5a) If $\lambda_{\text{tnt}} < \lambda$, accept the updates, i.e., $\lambda = \lambda_{\text{tnt}}$ and $\mathbf{v} = \mathbf{v}_{\text{tnt}}$, and return to Step 1.
- (5b) If $\lambda_{\text{tnt}} \geq \lambda$ and consecutive rejections of λ are less than n_{rpt} , accept only the eigenvector update, i.e., $\mathbf{v} = \mathbf{v}_{\text{tnt}}$, and return to Step 1.
- (5c) Otherwise, reduce the mesh size to 1/10, i.e., $r \leftarrow 0.1r$, and return to Step 1.

III. RESULTS

This work assesses the computation time needed to solve partial differential equations by using the proposed method with a given precision. Here, the computation time is evaluated by the number of iterations but not actual time. The purpose of the numerical experiments below is to investigate appropriate parameter settings. For this purpose, we prepare problems whose answers are known and modify the termination condition of the proposed algorithm. Although the algorithm stated in the previous section terminates when the precision r reaches a given value of the tolerance precision parameter ϵ_0 in the iterative descent stage, computation in the following terminates when the root mean squared error (RMSE) becomes less than the solution precision parameter ϵ_1 . Here, the true solution is defined by the solution of the corresponding SLE and is obtained by a classical linear equation solver.

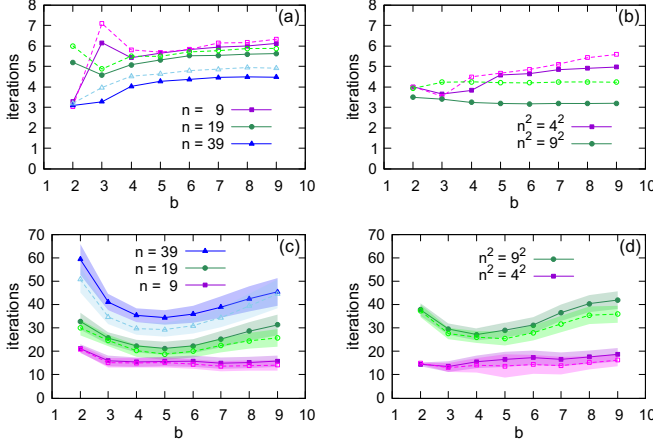


FIG. 1. The number of iterations at the initial guess (a and b) and iterative descent (c and d) stages for solving the one-dimensional (a and c) and two-dimensional (b and d) Poisson equations given by Eqs. (22) and (23), respectively. Symbols and shaded ranges illustrate the average and standard deviation, respectively. Annealing time is short for filled symbols with solid lines and long for open symbols with dashed lines.

The problems solved in this section are two kinds of Poisson equations. One is the one-dimensional Poisson equation defined as

$$-\frac{d^2}{dx^2}u(x) = f(x), \quad (22)$$

where $f(x) = -12x^2 + 12x - 2$ and $x \in [0, 1]$. The boundary condition is $u(x) = 0$ at $x = 0, 1$. The other one is the two-dimensional Poisson equation, defined as

$$-\left(\frac{\partial^2}{\partial x^2} + \frac{\partial^2}{\partial y^2}\right)u(x, y) = f(x, y), \quad (23)$$

where $f(x, y) = -2x(x-1) - 2y(y-1)$ and $x, y \in [0, 1]$. The boundary condition is $u(x, y) = 0$ at $x = 0, 1$ or $y = 0, 1$. The analytical solutions of Eqs. (22) and (23) are $u(x) = x^2(x-1)^2$ and $u(x, y) = xy(x-1)(y-1)$, respectively.

Here, we employ simulated annealing as an annealing procedure. Utilizing an Ising machine can shorten the computational time. However, it does not influence precision. In this section, the initial precision is taken as $r_{\text{init}} = 0.1$, and the solution precision parameter is $\epsilon_1 = 10^{-8}$. In this parameter setting, Step 5b of the iterative descent stage is unnecessary; thus, we set $n_{\text{rpt}} = 0$. Since our method includes a heuristic procedure, resulting in various computational times, we perform computation 10^3 times under each condition.

A. The number of iterations at each stage

Here, we see how the number of iterations depends on the precision parameter b and system size. When the

range $[0, 1]$ is discretized into $n+1$ slits in each dimension, system size, i.e., the dimension of vector \mathbf{u} of Eq. (4), is n for Eq. (22) and n^2 for Eq. (23). Figure 1 illustrates the number of iterations at each of initial guess and iterative descent stages for solving Eqs. (22) and (23). Filled symbols with solid lines and open symbols with dashed lines correspond to $N_s = 10^3$ and $N_s = 10^4$, respectively, where N_s denotes how many steps the temperature range is divided into and corresponds to an annealing time.

The difference in the number of iterations is small at the initial guess stage, as shown in Figs. 1(a) and 1(b). Filled and open symbols represent the average number of iterations for short and long annealing times, respectively. The standard deviation, which is not depicted, typically ranges from 0.5 to 1.5. In both one-dimensional (Fig. 1(a)) and two-dimensional (Fig. 1(b)) cases, the number of iterations required decreases as the system size increases and as the annealing time decreases.

Dependence on parameter b is significant in the iterative descent stage, especially for large- n cases. In both one-dimensional (Fig. 1(c)) and two-dimensional (Fig. 1(d)) cases, there is an optimal value of parameter b for each system size except for small-size systems. The larger the system size, the more iterations are required. A long annealing time lowers the number of iterations. However, even when the annealing time is increased by ten times, the number of iterations only reduces by about 10%. Therefore, we will take $N_s = 10^3$ to shorten the total computation time.

B. The number of precision updates

For setting the tolerance precision parameter ϵ_0 as appropriate, it is helpful to estimate how many times r changes at the iterative descent stage until obtaining a solution in a desirable precision ϵ_1 . The RMSE is evaluated for the solution vector \mathbf{u} given by Eq. (8). Errors in vector \mathbf{v} depend on n and b . Moreover, the eigenvalue λ depends on n . Balancing the desirable precision ϵ_1 with the RMSE, we can express how r depends on n and b . From the expression, whose derivation is given in Appendix A, the number of precision updates n_{upd} is estimated as

$$n_{\text{upd}} = \log_{10} \frac{r_{\text{init}}}{r} \simeq -(\log_{10} 2)b + \log_{10}(n - \alpha n^{1/2}) + \alpha', \quad (24)$$

where α and α' are coefficients.

Equation (24) implies that the number of precision updates decreases linearly with b and increases almost logarithmically with n . This behavior appears in Figs. 2(a) and 2(b). The equation solved for Fig. 2 is Eq. (22), and we here set $N_s = 10^3$ for saving computational time. While open symbols depict maximum numbers of updates, which are discrete numbers, filled symbols with solid lines are average numbers. The dashed lines in Fig. 2 demonstrate Eq. (24) with $\alpha = 2.7$ and $\alpha' = 7.9$,

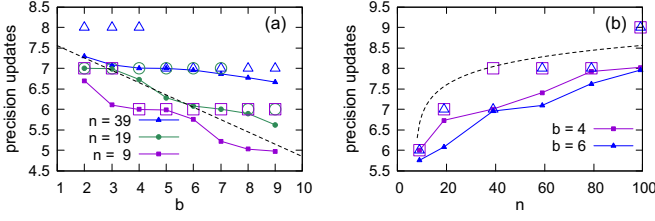


FIG. 2. The number of precision updates depending on the precision parameter b (a) and the system size n (b) for solving Eq. (22). The open symbols depict the maximum number of updates, and the filled symbols with solid lines illustrate the average numbers. The dashed lines in (a) and (b) show theoretical estimates given by Eq. (24) for $n = 9$ and $b = 4$, respectively.

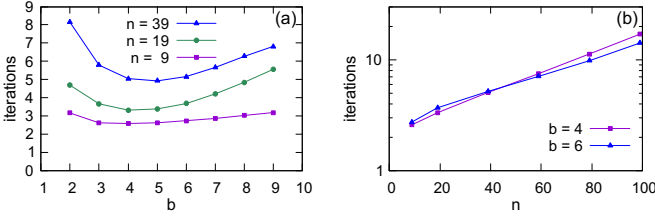


FIG. 3. The average number of iterations at each precision as a function of the precision parameter b (a) and the system size n (b) for solving Eq. (22).

which is determined by fitting Eq. (24) to the maximum numbers. Although the average number for $n = 39$ has a smaller slope than the dashed line in Fig. 2(a), the maximum number shows a similar slope to the dashed line. In Fig. 2(b), the maximum numbers for $b = 4$ and $b = 5$ are almost identical. Overall, the estimate given by Eq. (24) agrees well with the numerical results shown in Fig. 2.

C. The number of iterations at each precision

Figure 3 illustrates the average number of iterations at each value of r . Here, the equation solved is Eq. (22), and $N_s = 10^3$. Therefore, the values plotted in Fig. 3 multiplied by the average number of precision updates in Fig. 2 approximately equal the total number of iterations at the iterative descent stage. The curves in Fig. 3(a) look similar to the solid curves in Fig. 1(c).

In a large- b region, the number of iterations increases more rapidly in Fig. 3(a) than in Fig. 1(c), which implies that the decay in the number of precision updates shown in Fig. 2(a) relaxes the increase in the total number of iterations. In a small- b region, the number of iterations is also large and increases rapidly with the system size n . When mesh size is large, the adjusted difference vector has difficulty to take an optimal direction, which results in an ill convergence for small b . As b increases, the mesh size becomes fine, which may cause a good convergence. However, the dimension of a search space increases expo-

entially with b , which causes a worse convergence. The optimal value of b depends on the balance between the mesh size and search space dimension.

Figure 3(b) demonstrates that the number of iterations increases exponentially with n . This exponentially growing behavior also appears in the total number of iterations, which is not shown here. Although the difference between the results for $b = 4$ and $b = 6$ is small, the number of iterations for a larger b becomes smaller than that for a smaller b as n increases.

IV. DISCUSSION

The errors evaluated above are those in the SLE, although our original purpose is to solve PDEs. In reality, the discretization error is essential for solving a PDE. Denoting the interval as $h = n + 1$, the order of the discretization error is $O(h^2)$ in the central difference scheme. Thus, the tolerance precision parameter ϵ_0 for a small n may be set to a relatively large value. However, if one needs more accuracy in the solution of a PDE, n should be large.

In terms of implementation, the system size is essential, compared with the precision parameter. The number of iterations, i.e., computing time, increases exponentially with the system size for a given precision. On the other hand, an appropriate value of b can be determined for a given system size, as shown in Figs. 1 and 3(a).

In this paper, we have demonstrated results for solving relatively simple problems. Solving complicated problems should take more time. For setting appropriate parameters, it may be helpful to try computing the number of iterations and precision updates for several system sizes. One can estimate suitable parameter values by fitting the n_{upd} curve given by Eq. (24) to the obtained data.

V. CONCLUSIONS

In this work, we have assessed an annealing-based approach to solve PDEs. Our method is based on the algorithm initially proposed for solving eigenvalue problems proposed in Ref. [11]. This work has improved the algorithm for solving PDEs and provided a guideline for setting parameters to achieve efficient computing.

The examples demonstrated in this paper are for simple and small problems and show good performance. However, conventional methods can solve such a simple and small problem faster than the proposed one. Employing the proposed method with an Ising machine that can handle many variables can be promising for efficient computing for solving PDEs.

ACKNOWLEDGMENTS

This work was partially supported by a JSPS KAKENHI Grant Number JP23H04499.

Appendix A: Estimating the number of precision updates

Here, we estimate the number of precision updates. When \mathbf{v} , which is a unit vector, corresponds to the true solution, the error \mathbf{c} in the solution \mathbf{u} is approximately given as

$$\mathbf{c} = \frac{\lambda(\mathbf{v} + \mathbf{d})}{\tilde{\mathbf{f}}^\top(\mathbf{v} + \mathbf{d})} - \frac{\lambda\mathbf{v}}{\tilde{\mathbf{f}}^\top\mathbf{v}}, \quad (\text{A1})$$

where λ is the eigenvalue, and \mathbf{d} denotes the error in \mathbf{v} , and $\mathbf{d} \perp \mathbf{v}$. Supposing $\tilde{\mathbf{f}}^\top\mathbf{v} = \cos\theta_v$ and $\tilde{\mathbf{f}}^\top\mathbf{d} = (\cos\theta_d)d$, we have

$$c^2 = \|\mathbf{c}\|^2 = \frac{\lambda(\cos^2\theta_v + \cos^2\theta_d)d^2}{[\cos\theta_v + (\cos\theta_d)d]^2 \cos^2\theta_v}. \quad (\text{A2})$$

The RMSE is then described as

$$c = \frac{\lambda\beta_1 d}{\beta_2 + d}, \quad (\text{A3})$$

where $\beta_1 = \sqrt{\cos^2\theta_v + \cos^2\theta_d}/(\cos\theta_v \cos\theta_d)$, $\beta_2 = \cos\theta_v/\cos\theta_d$. Balancing the RMSE c with the desirable precision ϵ_1 leads to

$$d = \frac{\epsilon_1\beta_2}{\lambda\beta_1 - \epsilon_1}. \quad (\text{A4})$$

As mesh size for precision r is $2^{-b+1}r$, the hypercube's longest diagonal in the n -dimensional space is $2^{-b+1}rn^{1/2}$, corresponding to d . The eigenvalue $\lambda = (\mathbf{v}^\top A \mathbf{v})/(\mathbf{v}^\top B \mathbf{v})$ also depends on n . As $\|\mathbf{v}\| = 1$ and $A = -\tilde{\mathbf{f}}\tilde{\mathbf{f}}^\top$, where $\tilde{\mathbf{f}}$ is a unit vector, $\mathbf{v}^\top A \mathbf{v} \sim O(1)$. On the other hand, $\mathbf{v}^\top B \mathbf{v}$ corresponds to the discretization of $-\nabla^2$ divided by $\|\tilde{\mathbf{f}}\|$. While the Laplacian is almost independent of n , $\|\tilde{\mathbf{f}}\|$ is roughly proportional to $n^{1/2}$. Thus, $\mathbf{v}^\top B \mathbf{v} \sim O(n^{-1/2})$ results in $\lambda \sim O(n^{1/2})$. Considering $\lambda \propto n^{1/2}$ and $d = 2^{-b+1}rn^{1/2}$, we can rewrite Eq. (A4) into

$$r \simeq \frac{\epsilon_1\beta_2}{2^{-b+1}(\beta_3 n - \epsilon_1 n^{1/2})}, \quad (\text{A5})$$

where β_3 is the proportionality coefficient multiplied by β_1 . Then, the number of precision updates n_{upd} is estimated as

$$n_{\text{upd}} = \log_{10} \frac{r_{\text{init}}}{r} \simeq -(\log_{10} 2)b + \log_{10}(n - \alpha n^{1/2}) + \alpha', \quad (\text{A6})$$

where $\alpha = \epsilon_1/\beta_3$ and $\alpha' = 2r_{\text{init}}\beta_3/(\epsilon_1\beta_2)$.

-
- [1] Y. Cao, A. Papageorgiou, I. Petras, J. Traub, and S. Kais, Quantum algorithm and circuit design solving the Poisson equation, *New J. Phys.* **15**, 013021 (2013).
 - [2] A. M. Childs, J.-P. Liu, and A. Ostrander, High-precision quantum algorithms for partial differential equations, *Quantum* **5**, 574 (2021).
 - [3] H.-L. Liu, Y.-S. Wu, L.-C. Wan, S.-J. Pan, S.-J. Qin, F. Gao, and Q.-Y. Wen, Variational quantum algorithm for the Poisson equation, *Phys. Rev. A* **104**, 022418 (2021).
 - [4] Y. Sato, R. Kondo, S. Koide, H. Takamatsu, and N. Imoto, Variational quantum algorithm based on the minimum potential energy for solving the Poisson equation, *Phys. Rev. A* **104**, 052409 (2021).
 - [5] Y. Y. Liu, Z. Chen, C. Shu, S. C. Chew, B. C. Khoo, X. Zhao, and Y. D. Cui, Application of a variational hybrid quantum-classical algorithm to heat conduction equation and analysis of time complexity, *Phys. Fluids* **34**, 117121 (2022).
 - [6] R. Demirdjian, D. Gunlycke, C. A. Reynolds, J. D. Doyle, and S. Tafur, Variational quantum solutions to the advection–diffusion equation for applications in fluid dynamics, *Quantum Inf. Proc.* **21**, 322 (2022).
 - [7] C. Bravo-Prieto, R. LaRose, M. Cerezo, Y. Subasi, L. Cincio, and P. J. Coles, Variational Quantum Linear Solver, *Quantum* **7**, 1188 (2023).
 - [8] Y. Sato, H. C. Watanabe, R. Raymond, R. Kondo, K. Wada, K. Endo, M. Sugawara, and N. Yamamoto, Variational quantum algorithm for generalized eigenvalue problems and its application to the finite-element method, *Phys. Rev. A* **108**, 022429 (2023).
 - [9] A. Teplukhin, B. K. Kendrick, and D. Babikov, Calculation of Molecular Vibrational Spectra on a Quantum Annealer, *J. Chem. Theor. Comp.* **15**, 4555 (2019).
 - [10] A. Teplukhin, B. K. Kendrick, S. Tretiak, and P. A. Dub, Electronic structure with direct diagonalization on a D-wave quantum annealer, *Sci. Rep.* **10**, 20753 (2020).
 - [11] B. Krakoff, S. M. Mniszewski, and C. F. A. Negre, Controlled precision QUBO-based algorithm to compute eigenvectors of symmetric matrices, *PLOS ONE* **17**, e0267954 (2022).
 - [12] M. W. Johnson, M. H. S. Amin, S. Gildert, T. Lanting, F. Hamze, N. Dickson, R. Harris, A. J. Berkley, J. Johansson, P. Bunyk, E. M. Chapple, C. Enderud, J. P. Hilton, K. Karimi, E. Ladizinsky, N. Ladizinsky, T. Oh, I. Perminov, C. Rich, M. C. Thom, E. Tolkacheva, C. J. S. Truncik, S. Uchaikin, J. Wang, B. Wilson, and G. Rose, Quantum annealing with manufactured spins, *Nature* **473**, 194 (2011).
 - [13] M. Yamaoka, C. Yoshimura, M. Hayashi, T. Okuyama, H. Aoki, and H. Mizuno, A 20k-spin Ising chip to solve combinatorial optimization problems with CMOS annealing, *IEEE J. Solid-State Circ.* **51**, 303 (2016).
 - [14] K. Yamamoto, W. Huang, S. Takamaeda-Yamazaki,

- M. Ikebe, T. Asai, and M. Motomura, A time-division multiplexing Ising machine on FPGAs, in *Proceedings of the 8th International Symposium on Highly Efficient Accelerators and Reconfigurable Technologies*, HEART2017 (Association for Computing Machinery, New York, NY, USA, 2017).
- [15] Y. Kihara, M. Ito, T. Saito, M. Shiomura, S. Sakai, and J. Shirakashi, A new computing architecture using Ising spin model implemented on FPGA for solving combinatorial optimization problems, in *2017 IEEE 17th International Conference on Nanotechnology (IEEE-NANO)* (2017) pp. 256–258.
- [16] .
- [17] T. Okuyama, T. Sonobe, K.-i. Kawarabayashi, and M. Yamaoka, Binary optimization by momentum annealing, *Phys. Rev. E* **100**, 012111 (2019).
- [18] S. Matsubara, M. Takatsu, T. Miyazawa, T. Shibasaki, Y. Watanabe, K. Takemoto, and H. Tamura, Digital Annealer for high-speed solving of combinatorial optimization problems and its applications, in *2020 25th Asia and South Pacific Design Automation Conference (ASP-DAC)* (2020) pp. 667–672.
- [19] K. Yamamoto, K. Ando, N. Mertig, T. Takemoto, M. Yamaoka, H. Teramoto, A. Sakai, S. Takamaeda-Yamazaki, and M. Motomura, STATICA: A 512-spin 0.25M-weight full-digital annealing processor with a near-memory all-spin-updates-at-once architecture for combinatorial optimization with complete spin-spin interactions, in *2020 IEEE International Solid-State Circuits Conference (ISSCC)* (2020) pp. 138–140.
- [20] H. Goto, K. Tatsumura, and A. R. Dixon, Combinatorial optimization by simulating adiabatic bifurcations in nonlinear Hamiltonian systems, *Sci. Adv.* **5**, eaav2372 (2019).
- [21] K. Tatsumura, R. Hidaka, M. Yamasaki, Y. Sakai, and H. Goto, A currency arbitrage machine based on the simulated bifurcation algorithm for ultrafast detection of optimal opportunity, in *2020 IEEE International Symposium on Circuits and Systems (ISCAS)* (IEEE, Seville, Spain, 2020) pp. 1–5.
- [22] H. Goto, K. Endo, M. Suzuki, Y. Sakai, T. Kanao, Y. Hamakawa, R. Hidaka, M. Yamasaki, and K. Tatsumura, High-performance combinatorial optimization based on classical mechanics, *Sci. Adv.* **7**, eabe7953 (2021).
- [23] R. Hidaka, Y. Hamakawa, J. Nakayama, and K. Tatsumura, Correlation-Diversified Portfolio Construction by Finding Maximum Independent Set in Large-Scale Market Graph, *IEEE Access* **11**, 142979 (2023).
- [24] Z. Wang, A. Marandi, K. Wen, R. L. Byer, and Y. Yamamoto, Coherent Ising machine based on degenerate optical parametric oscillators, *Phys. Rev. A* **88**, 063853 (2013).
- [25] A. Marandi, Z. Wang, K. Takata, R. L. Byer, and Y. Yamamoto, Network of time-multiplexed optical parametric oscillators as a coherent Ising machine, *Nature Photonics* **8**, 937 (2014).
- [26] T. Inagaki, Y. Haribara, K. Igarashi, T. Sonobe, S. Tamate, T. Honjo, A. Marandi, P. L. McMahon, T. Umeki, K. Enbutsu, O. Tadanaga, H. Takenouchi, K. Aihara, K. Kawarabayashi, K. Inoue, S. Utsunomiya, and H. Takesue, A coherent Ising machine for 2000-node optimization problems, *Science* **354**, 603 (2016).
- [27] P. L. McMahon, A. Marandi, Y. Haribara, R. Hamerly, C. Langrock, S. Tamate, T. Inagaki, H. Takesue, S. Utsunomiya, K. Aihara, R. L. Byer, M. M. Fejer, H. Mabuchi, and Y. Yamamoto, A fully programmable 100-spin coherent Ising machine with all-to-all connections, *Science* **354**, 614 (2016).
- [28] R. Hamerly, T. Inagaki, P. L. McMahon, D. Venturelli, A. Marandi, T. Onodera, E. Ng, C. Langrock, K. Inaba, T. Honjo, K. Enbutsu, T. Umeki, R. Kasahara, S. Utsunomiya, S. Kako, K.-i. Kawarabayashi, R. L. Byer, M. M. Fejer, H. Mabuchi, D. Englund, E. Rieffel, H. Takesue, and Y. Yamamoto, Experimental investigation of performance differences between coherent Ising machines and a quantum annealer, *Sci. Adv.* **5**, eaau0823 (2019).
- [29] Z. Zhong and F. You, Globally convergent exact and inexact parametric algorithms for solving large-scale mixed-integer fractional programs and applications in process systems engineering, *Comp. Chem. Eng.* **61**, 90 (2014).